AD 728362

(1)

NATIONAL RESEARCH COUNCIL OF CANADA

MECHANICAL ENGINEERING REPORT
MT-61

A STUDY OF FLOW PHENOMENA IN EXTERNALLY PRESSURIZED GAS THRUST BEARINGS

by

I. R. G. LOWE
DIVISION OF MECHANICAL ENGINEERING

OTTAWA
DECEMBER 1970

NRC NO. 11918

43

A STUDY OF FLOW PHENOMENA IN EXTERNALLY PRESSURIZED GAS THRUST BEARINGS

by

I.R.G. LOWE

A.J. Bachmeier, Head
Gas Dynamics Section

D.C. MacPhail
Director

BLANK PAGE

SUMMARY

An experimental study of an externally pressurized, gas-lubricated, circular thrust bearing with central admission and operating in the inherent compensation mode is reported. Gas supply pressures covered the range from 1.25 to 4.0 atmospheres (absolute) while clearances varied from 0.0005 inch to 0.005 inch. Three feed-hole radius to bearing radius ratios were investigated: 0.0156, 0.0313, and 0.3. The effect of recess depth was also examined. The film entrance pressure loss has been shown to be a function of several bearing parameters, and an empirical orifice discharge coefficient equation was used to predict load and flow curves for a bearing.

TABLE OF CONTENTS

APPENDICES

ILLUSTRATIONS

SYMBOLS

Symbol	Definition	Units
a	Area	L^2
A	Bearing area $= \pi r_1^2$	L^2
c	Speed of sound	LT^{-1}
c^*	Speed of sound at Mach number $= 1$	LT^{-1}
C_d	Orifice discharge coefficient	
F_Q	Bearing flow coefficient	
F_W	Bearing load coefficient	
g	Gravitational constant	LT^{-2}
h	Clearance	L
k	Ratio of specific heats	
K	Entrance pressure drop factor	
Kg	$(p_i - p_a)/(p_s - p_a)$	
$\dot{m}$	Gas flow rate	FT^{-1}
M_i	Mach number at entrance to clearance space $= V_m/c$	
M^*	Mach number relative to speed of sound at $M = 1$	
N_{Re}	Reynolds number	
p	Pressure	FL^{-2}
p_e	Static pressure after isentropic acceleration	FL^{-2}
p_o	Pressure at r_s for load equalization model	FL^{-2}
p_{dyn}	Kinetic pressure at r_s	FL^{-2}
p^*	Static pressure related to a Mach number equal to 1	FL^{-2}
P	Normalized pressure (p/p_a)	
Q	Volumetric flow rate	L^3T^{-1}
r	Radius	L

SYMBOLS (Cont'd)

Symbol	Definition	Units
r_s	Radius of supply hole	L
r_1	Bearing outer radius	L
R_s	r_s/r_1	
Rg	Gas constant	$L\theta^{-1}$
T_s	Temperature of supply gas	θ
V_m	Mean gas velocity	LT^{-1}
ρ	Specific weight of gas	FL^{-3}
μ	Viscosity	FTL^{-2}
κ	Orifice discharge coefficient geometrical factor	
σ	$\sqrt{\dfrac{2 \log_e (1/R_s)}{1 - (1/P_o)^2}}$	

Subscripts refer to the following conditions:

o	ambient
i	film entrance
s	supply
c	critical

BLANK PAGE

A STUDY OF FLOW PHENOMENA IN EXTERNALLY PRESSURIZED GAS THRUST BEARINGS

1.0 INTRODUCTION

In order that a gas-lubricated bearing possess stiffness the gas must be fed into the clearance space through a flow restrictor. This restriction may take the form of an orifice, a capillary, a porous bearing wall, or a control device. Bearings, are often designed with what is termed inherent compensation, in which case the gas flow is restricted by the curtain area at the edge of the supply recess. The advantages of inherently-compensated bearings over the orifice-compensated type are their better stability characteristics and relative ease of manufacture.

Recently, in this laboratory, several bearing applications have been forthcoming that involved unchanging but large loads necessitating large bearing surfaces with consequently large clearances and high flow rates. For these circumstances inherently-compensated feeding holes optimized for minimum pumping power are also large. Initial tests with scaled models showed that instabilities could develop with this type of thrust bearing despite the fact that the inlet curtain area was at least ten times smaller than other restricting areas in the system. A study of the flow phenomena in such bearings was of obvious interest.

Several other researchers have studied flows in thrust bearings because of uncertainty in the analytical methods used to treat these flows (Ref. 1 to 11). The flow through the feeding recess curtain area has been treated until recently by the orifice equation. This equation, however, assumes a total loss of dynamic head downstream of the orifice and this has not been found to be the case (Ref. 6). Supersonic flow and shock wave phenomena are also known to occur in the feeding region of gas bearings, further complicating the analytical treatment (Ref. 8). Recently, Vohr (Ref. 6, 9) has suggested a method of correlating the pressure drop across the edge of the feeding holes in terms of a dynamic head factor as used commonly for entrance losses for flow in pipes.

Vohr's work has been extended somewhat by work at the Franklin Institute (Ref. 10); however, agreement has not been complete, and both reports have suggested that further work is needed to determine any systematic variations of the scatter in the results (see Fig. 1).

The experimental work described in this report has been undertaken with the twofold aim of confirming and extending the correlation of Vohr, especially as it may apply to inherently-compensated bearings with large feeding recesses, and also to determine stability derivatives for this type of bearing. This latter phase of the work will be reported separately.

2.0 EXPERIMENTAL DETERMINATION OF THRUST BEARING PRESSURE DISTRIBUTIONS

2.1 General Description

The experimental apparatus is shown in Figure 2. A circular thrust pad, 2 inches in diameter, with a single central feeding hole, moves over a 6-inch diameter lower block, as shown in Figures 3 and 4a. Figure 4b is a schematic representation of the apparatus. The two blocks were fabricated from 17-4-PH stainless steel and then hardened to Rockwell C47. The upper and lower bearing faces were ground, lapped, and polished flat to within a quarter of a wavelength of Helium light ($\simeq$ 4 micro-inches).

A brass plug was let into the hardened surface of the upper block to permit systematic changes in the feeding geometry. Bottled nitrogen, used for all the experimentation, was fed into the top of the upper block then through the feeding restrictor into the clearance space. The height of the clearance space was measured by three capacitance-type distance measuring probes and was set by three differential-screw legs on which the upper block slid over the lower.

The upper bearing block horizontal movement was measured by a dial indicator (Starrett 656-F 1 inch) in the longitudinal direction, and was restricted laterally by flat plates that served as guides for ground and lapped flats on the sides of the bearing block. A travelling microscope was used to position the lateral retaining plates so that the centre line of the feeding hole passed over a 0.001-inch diameter pressure tap in the centre of the base plate. Coincidence of the axes of the feeding hole and the pressure tap could also be confirmed, to within 0.00025 inch, by locating the point of maximum pressure in the pressure tap with a small (0.004-inch diameter) orifice inserted in the feeding hole.

The 0.001-inch diameter pressure tap hole was drilled into a brass plug (diameter = 3/16 inch) set into the lower bearing face. A pressure transducer was set into the lower block underneath the pressure tap so as to provide a dead space approximately 0.001 inch deep. This allowed rapid response by the pressure transducer. The waiting time between readings was of the order of one minute.

Vertical movement of the upper block due to the pressure in the clearance space was avoided by a spring-loaded arm acting through a steel ball resting in a conical cavity in the top of the slider. Clearance height could be maintained to within ± 30 micro-inches.

2.2 Capacitance Distance Measuring Probes

Capacitance probes for maximum gaps of 0.001 inch and 0.010 inch have been fabricated in accordance with the design procedure set out in the Wayne-Kerr Distance Meter Handbook. One of these probes is shown in Figure 5. A vee-block and a flat pad made to allow accurate calibration of these small probes are shown in Figure 6. In these pieces flatness, parallelism and perpendicularity tolerances were kept as small as possible. (All experimentation was conducted in a laminar flow work area of a temperature-controlled clean room.)

2.3 Pressure Measurement

Gas supply pressure was read on one of a series of manometers, as shown in Figure 2. Fine adjustment to the required supply pressure prior to reading the pressure at each radial position was made by means of a needle valve upstream of the flowrator.

Statham pressure transducers were employed under the pressure tap in the lower bearing block, as stated previously. Their sensitivities were ± 5 psid, 10 psid, 25 psid, and 50 psid. Each gauge was calibrated "in situ" by the use of a pressurized chamber held centrally over the pressure tap by the loading bridge. The pressure in the cell was measured by manometer, while the gauge output was recorded on a potentiometric recorder. The excitation voltage for the gauge was provided by dry cell batteries through a potential divider circuit. A precision resistor in the divider circuit allowed accurate measurement of the excitation voltage.

2.4 Gas Flow Measurement

Bottled nitrogen, of commercial purity, was used for all tests. The gas passed through a pressure regulator and high quality filter before measurement by Kontes precision flowmeters. The flowmeters were calibrated by a water displacement technique, confirmed by a Sargent Wet Test gas meter, and allowed a flow measurement accuracy of better than 2 percent. Measured flow rates were compared with theoretical flow rates, calculated using the measured clearance and pressure as discussed in the following Section.

3.0 ANALYSIS OF RESULTS

3.1 Flow Equations

The equation describing radial, compressible, isothermal, viscous flow between two plates has been used to calculate the bearing flow rates from measured values of clearance, h, and pressure, p, at any radius, r, i.e.

$$p^2 - p_a^2 = \frac{12\mu R_g T_s \dot{m}}{\pi h^3} \log_e(r_1/r) \qquad (1)$$

where T_s is the ambient temperature as the flow is isothermal.* Vohr (Ref. 6) made a correction for inertia effects in the flow by subtracting the mean dynamic pressure $(1.2\,\rho V_m{}^2/2g)$ from the pressure given by the above equation. This method of correction has been used for the results reported here.

3.2 Correlation of Entrance Pressure Drop

The correlation of entrance pressure loss proposed by Vohr assumes that the gas is accelerated isentropically from stagnation conditions in the feeding hole to

---

* A complete derivation of this equation is given in Reference 5.

fill the whole clearance space, i.e. with no vena contracta present. The resulting dynamic pressure is then correlated by

$$K\, p_{dyn} = \text{entrance pressure loss} = p_s - p_i \qquad (2)$$

where p_i is the pressure that would exist at the entrance to the clearance space if equation (1) applied to the whole region, i.e. $p = p_i$ for $r = r_s$, and p_s is the supply pressure - the stagnation pressure in the feeding hole.

The dynamic pressure is a function of the Mach number since

$$p_{dyn} = p_s - p_e \qquad (3)$$

and (see Ref. 15)

$$\frac{p_e}{p_s} = \frac{p_e}{p^*} \times \frac{p^*}{p_s} = \left[\frac{k+1}{2(1 + \frac{k-1}{2} M_i^2)}\right]^{k/k-1} \times \left[\frac{k+1}{2}\right]^{-k/k-1} \qquad (4)$$

which for nitrogen becomes

$$\frac{p_e}{p_s} = 0.528 \left[\frac{1.2}{1 + 0.2\, M_i^2}\right]^{3.5} \qquad (5)$$

Following Vohr, we have also

$$M^* \frac{\rho}{\rho_s} = \frac{\dot{m}}{c^* a_i \rho_s} = 0.634 M_i \left[\frac{1.2}{1 + 0.2\, M_i^2}\right]^3 \text{ for nitrogen} \qquad (6)$$

and this may be expressed as the polynomial

$$M_i^6 + 15\, M_i^4 + 75\, M_i^2 - \frac{137 \cdot c^* a_i \rho_s}{\dot{m}} M_i + 125 = 0 \qquad (7)$$

3.3 Computational Analysis

A Fortran IV program was written to analyze the experimental data and a complete transcription is appended. The pressure measurements were integrated to give the bearing load capacity, and equation (1) was solved for several radii near the outside of the bearing where inertia effects could be handled by the approximation mentioned in Section 3.1. The averaged flow rates calculated at several radii were compared with the measured flow rate as a test of the experimental method.

The measured flow and clearance were substituted into equation (1) along with the radius of the feeding hole, r_s, to give a value for the pressure at r_s, which was termed p_i, the pressure that would exist at r_s if inertia effects were negligible and the flow was everywhere viscous. The resultant pressure, p_i, was used to calculate the well-known gas-bearing pressure ratio Kg where

$$Kg = \frac{p_i - p_o}{p_s - p_o} \tag{8}$$

The measured flow rate was also used in the calculation of the entrance Reynolds number, $\dot{m}/\pi\ r_s\ \mu g$. An equivalent orifice discharge coefficient was then found assuming that the orifice pressure drop was the difference between the supply pressure, p_s, and the pressure at the entrance to the clearance space, p_i. It was also assumed that the orifice area was equal to the inherent restrictor area, $2\pi\ r_s\ h$, or

$$C_d = \frac{\dot{m}}{2\pi r_s h \left[p_s \cdot 2g\rho_s \left(\frac{k}{k-1}\right)\left(\left(\frac{p_i}{p_s}\right)^{2/k} - \left(\frac{p_i}{p_s}\right)^{\frac{k-1}{k}}\right)\right]^{1/2}} \tag{9}$$

Equation (7) was then solved by the Newton-Raphson iterative technique using the IBM scientific subroutine POLRT. As there are two real roots to the equation, the subsonic and supersonic solutions, the pressure profiles in the entrance region were examined for pressures less than the critical pressure, $0.528\ p_s$, in which case the supersonic Mach number was selected. The static pressure at the entrance was next computed from equation (5) and consequently the dynamic pressure, p_{dyn}, and the entrance pressure drop factor, K.

4.0 RESULTS

4.1 Extent of Tests

Pressure profile measurements were carried out for values of R_s equal to 0.01563, 0.03125, and 0.3, while supply pressure ratios were varied from 1.25 to 4.0. Clearances ranged from 0.0005 inch to 0.005 inch.

4.2 Pressure Distributions

Several features of the experimental set-up have combined to allow pressure distribution measurements of very high accuracy. The pressure tap hole of 0.001-inch diameter resulted in good spatial resolution, while the pressure transducer with minimum "dead space" avoided long delays for pressure equilibration. Figures 7 shows three of the pressure profiles taken at a feeding-hole radius ratio of 0.03125 and a supply pressure ratio of 2.0. Illustrated here is the well-known change of pressure profile with clearance, ranging from a nearly completely viscous case, to the case where inertia effects are marked, and then to the supersonic flow pattern with one or more shock waves standing in the clearance space. Superimposed on the experimental points are the theoretical curves of equation (1), with inertia correction, using the measured flow rates and measured clearances. As stated earlier, a mean flow rate was calculated in each case using several pressure measurements at the outer radii in equation (1). Agreement between the calculated and measured flows of within ± 6 percent was considered acceptable.

4.3 Effect of Supply Pressure

The effects of several variables were investigated and the results of these will now be discussed. In Figures 8 and 9 the effect of supply pressure ratio on bearing pressure distribution is shown at different clearance heights. For a clearance of 0.001 inch (Fig. 8), the bearing entrance pressure drop increases with supply pressure, as would be expected, because of the increasing mass flow rate.

The effect of the increasing mass flow rate on the kinetic component of the pressure is quite noticeable at a supply pressure of 2.5 atmospheres. The pressure distribution shows a recovery of static head as the mean flow velocity decreases with increasing radius.

The effect of supply pressure at a clearance of 0.004 inch is shown in Figure 9, plotted on expanded scales for clarity. It can be seen that the minimum pressure attained decreases and the subatmospheric region extends to larger radii as the supply pressure increases. The nearly vertical pressure jumps for the three higher pressure ratio cases are probably due to shock waves standing in the clearance space, although the probability of this phenomenon is still a matter of discussion (see, for example, McCabe et alia, Ref. 10, p. 36).

Some confirmation of the presence of a shock wave is obtained by applying supersonic flow theory in the manner of Mori (Ref. 8). This is illustrated in Figure 10. The experimental pressures at $r = 0.10$ agree very closely with the theoretical inertially corrected viscous profile. Using the matching criterion of Vohr, Reference 9, that the after-shock pressure match the viscous-inertial profile, the shock position is slightly downstream of the position it would have if the total pressure or purely viscous profile (eq. (1)) were matched with the after-shock pressure. In either case the theoretical shock position agrees quite adequately with the steeply rising portion of the pressure profile that was previously said to indicate a shock position. It was also found when recording profiles such as shown in Figure 10, that the pressures in the radius range 0.06 to 0.09 showed fluctuations of the order of $\pm$ 2 percent.

4.4 Effect of Recess Depth

Other work in this laboratory by E.H. Dudgeon (Ref. 14) has shown how an optimization of the pumping power requirement for a bearing may lead to feeding-hole diameters that are quite large. For this reason we studied not only large single diameter feeding holes but also feeding holes with recesses, where the edge of the recess was the main flow restrictor. Figure 11 shows the variation of the entrance region pressure profile with recesses of different depth. For a gap height of 0.001 inch the bearing is inherently compensated and the supply pressure extends nearly to the edge of the recess. A slight orifice effect at the feeding hole is noticeable for the smallest recess depth (0.005 inch). In this case the ratio of orifice area to the inherent restriction area at the edge of the feeding hole (not the recess) is slightly less than one.

For the large clearance cases an orifice pressure drop is present for all recess depths since the orifice area and inherent restriction area of the recess ($2\pi\ r_s\ h$) are now nearly equal. The larger recess depth bearings establish a steady "post-orifice" pressure over a smaller outer portion of the recess, but this is not evident with the smallest recess depth, where the flow from the orifice does not "notice" the recess at all. It is important, then, when designing recessed bearings that an operating clearance is chosen, and maintained, that ensures operation as an inherently-compensated bearing at all times.

4.5 Large Radius Ratio Supply Holes

As previously mentioned, inherently-compensated bearings with large radius ratio supply holes are of interest when compressor power requirements are optimized. It is also possible that a pressure depression at the edge of a large radius ratio supply hole could affect the bearing's stability. A series of tests was made with a second upper block assembly (see Fig. 12) having a supply hole diameter of 0.6 inch, i.e., a radius ratio of 0.3. This ratio was chosen to be the same as that for another, larger diameter bearing being used for stability studies. Figures 13, 14, and 15 show the resulting pressure distributions.

In general, the same pressure distribution shapes were found as for the smaller radius ratio cases. The adverse pressure gradients due to the inertial pressure component are again evident. Because of the large supply-hole radius, the cross-sectional area at the entrance to the clearance space is large and sub-critical pressures occur only at the largest flow rates.

In contrast to the lower radius ratio tests, where the measured and calculated flows in general agreed quite well, the flow measurements for the large radius ratio tests showed a consistently increasing disagreement with the calculated values. This can be seen in Figure 16, where the disagreement between calculated and measured flow is plotted against entrance Reynolds number. The trend is for the calculated flow, based on equation (1) with inertia correction, to become increasingly larger than the measured flow rate as that measured flow rate (expressed as entrance Reynolds number) increases. This indicates the inadequacy of the inertial-viscous flow model under flow conditions that are almost certainly turbulent. The critical Reynolds number for reverse transition from turbulent to laminar flow has been discussed by several authors, whose findings are summarized by McCabe et alia in Reference 10. The criterion of Chen and Peube (Ref. 12), as verified experimentally by Kreith (Ref. 13), is that

$$\frac{r_c}{h} = 0.35 \sqrt{\frac{r_i}{h}} \sqrt{N_{Re}}$$

where r_c is the minimum radial distance for reverse transition. If we examine

Figure 16 and select an entrance Reynolds number of 2000 as the maximum at which measured and calculated flows are in agreement, we have

$$r_c \simeq 8.6\ h^{1/2}$$

Thus, choosing $h = 0.002$ inch as representative of the maximum h for Reynolds numbers less than 2000, we have $r_c \simeq 0.4$ inch. For higher Reynolds numbers the turbulent zone will extend even farther and calculations based on the laminar flow equations will be increasingly inaccurate. (Chen and Peube in fact suggested that the flow does not become completely laminar until the inertia terms are very small.)

4.6 Entrance Pressure Drop Correlation

Figure 17 summarizes the entrance pressure drop information obtained during these tests. The results of tests at a radius ratio of 0.3 that were not reasonably well fitted to the viscous-inertial flow curve have been omitted. Also shown, as black squares, are the experimental points reported by McCabe et alia, Reference 10. Several probable error estimates are shown, since it is increasingly difficult experimentally to keep the error in K small as the clearance and Reynolds number are reduced. Points lying to the right of the dashed curve represent cases where the pressure in the entrance region was subcritical and consequently Mach numbers were greater than 1.0 for the calculation of the dynamic pressure. It is evident that the simple Reynolds number correlation of Reference 6 is not adequate. In addition, the extreme difficulty of making accurate measurements of the small difference $p_s - p_i$ at low Reynolds numbers precludes the use of this correlation over a large part of the subsonic range.

Dudgeon, in Reference 14, has shown how the bearing entry pressure drops may be treated in terms of a variable orifice coefficient

$$C_d = \kappa \left(\frac{P_o}{P_s}\right) \left(P_o^{\,2} - 1\right)^{0.2} \ \frac{h}{r_s}^{0.56} \tag{10}$$

where κ is a factor depending on supply-hole radius, r_s, and the radius ratio, R_s. κ can be read from Figure 18, which is reproduced from Reference 14. The pressure ratio P_o is equal to p_o/p_a where p_o is the pressure at the entrance to the clearance space for a purely viscous pressure profile that has a load capacity equal to the actual bearing load capacity.

Figure 19 compares theoretical and measured load and flow curves for an R_s of 0.0313 and a supply pressure ratio, P_s, of 2. The analytical method used to calculate loads and flows is described in Appendix B. The agreement between calculations and experiment is more than adequate for design purposes especially at the design point, $Kg = 0.65$, chosen for maximum stiffness as well as optimum radius ratio.

5.0 CONCLUSIONS

It has been demonstrated that over a wide range of radius ratios and supply pressures the entrance pressure losses are functions not only of film entrance Reynolds number, but also of clearance height to recess radius ratio, supply pressure ratio, and film entrance pressure ratio. An empirical orifice discharge coefficient equation involving these parameters allows adequately accurate prediction of loads and flows for centrally-fed, inherently-compensated, thrust bearings. It is recommended that the entrance Reynolds number be kept low enough that flow be laminar over the outer half of the bearing, i.e. for all $r > r_1/2$, hence the viscous-inertial flow model can apply.

6.0 REFERENCES

1. Mori, H. — A Theoretical Investigation of Pressure Depression in Externally Pressurized Gas-Lubricated Circular Thrust Bearings. J. Basic Engrg., Trans. ASME, Vol. 83D, 1961, pp. 201-208.

2. Gross, W.A. — Gas Film Lubrication. Chapter 5. John Wiley and Sons, Inc., New York, 1962.

3. Mori, H., Miyamatsu, Y., Sakata, S. — Research on Externally Pressurized Circular Thrust Gas-Lubricated Bearings. Bull. of Japan Soc. Mech. Engrs. Vol. 7, 1964, pp. 467-473.

4. Mori, H., Sakata, S. — Observation of Compressible Flow Between Circular and Parallel Plates (A Contribution to Externally Pressurized Circular Thrust Bearings). Lubrication, Vol. 10, 1965, pp. 435-441.

5. Carfagno, S.P., McCabe, J.T. — Summary of Investigations of Entrance Effects in Circular Thrust Bearings. The Franklin Institute Research Laboratories, Interim Report I-A2049-24, Philadelphia, Pa., August 1965.

6. Vohr, J.H. — An Experimental Study of Flow Phenomena in the Feeding Region of an Externally Pressurized Gas Bearing. Mechanical Technology Inc., Report MTI-65TR47, Latham, New York, July 21, 1966.

7. Carfagno, S.P. — An Analysis of Experimental Data on Entrance Effects in Circular Thrust Bearings. The Franklin Institute Research Laboratories, Interim Report I-A2049-28, Philadelphia, Pa., September 1966.

8. Mori, H., Miyamatsu, Y. — Theoretical Flow-Models for Externally Pressurized Gas Bearings. Trans. of ASME., J. of Lubrication Technology, Vol. 91, Series F, No. 1, January 1969, pp. 181-193.

9. Vohr, J.H. — A Study of Inherent Restrictor Characteristics for Hydrostatic Gas Bearings. Gas Bearing Symposium, Paper No. 30, University of Southampton, April 1969.

10. McCabe, J.T., Elrod, H.G., Carfagno, S., Colsher, R. — Summary of Investigations of Entrance Effects of Circular Thrust Bearings. Gas Bearing Symposium, Paper 17, University of Southampton, April 1969; also Franklin Institute Research Laboratories Interim Report I-C2429-1, Philadelphia, Pa., November 1969.

11. Okrouhlík, M. — Theoretical and Experimental Investigation of Pressure Distribution in Gas Lubricated Circular Thrust Bearings. École Polytechnique, Montreal; M.A.Sc. Thesis, Department of Mechanics, August 1969.

12. Chen, C.P., Peube, J.L. — Sur l'Écoulement Radial Divergent d'un Fluide Visqueux Incompressible entre Deux Plans Parallèles. Comptes Rendues, Acad. Sc. Paris, 258, Groupe 2, 1964, pp. 5353-5355.

13. Kreith, F. — Reverse Transition in Radial Source Flow Between Two Parallel Planes. Physics of Fluids, Vol. 8, 1965, pp. 1189-1190.

14. Dudgeon, E.H. — Performance Factors for Circular, Hydrostatic, Gas-Lubricated Thrust Bearings, Part I. NRC, DME Mech. Eng. Report MT-62, National Research Council of Canada, Ottawa, 1970.

15. Keenan, J.H., Kaye, J. — Gas Tables. John Wiley and Sons, Inc., New York, 1948.

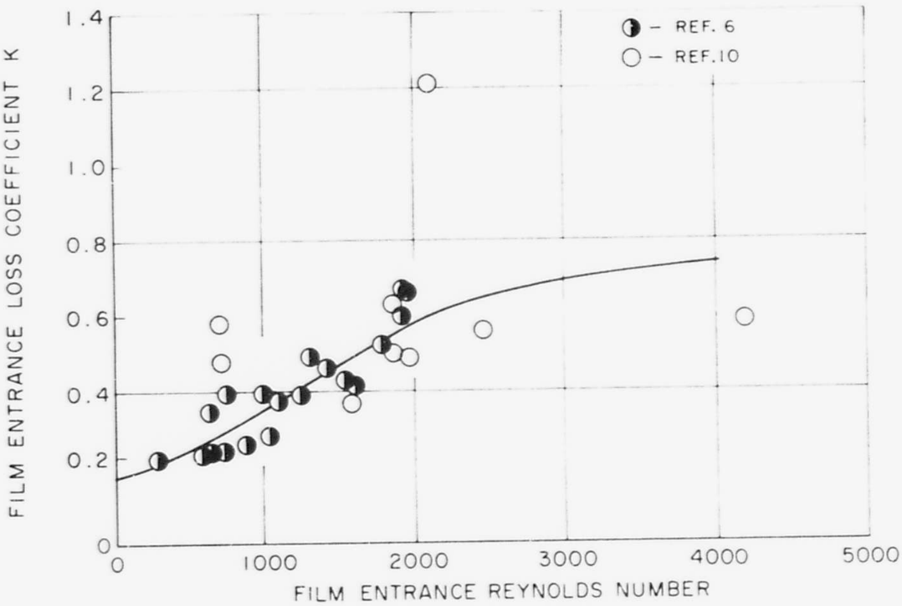

FIG. 1 : ENTRANCE LOSS CORRELATION DUE TO VOHR (REF. 6) AS EXTENDED BY McCABE, et alia, (REF. 10)

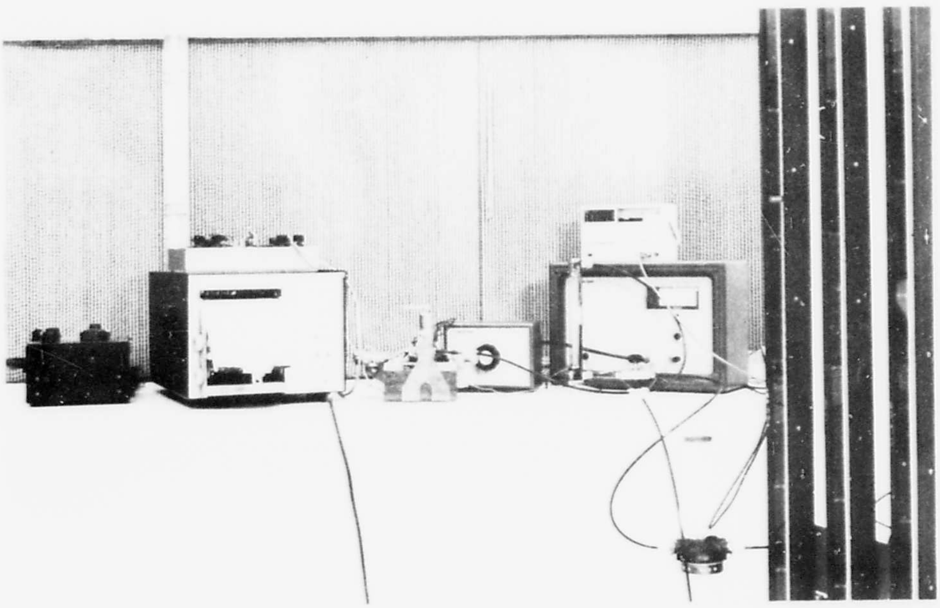

FIG. 2 : EXPERIMENTAL APPARATUS

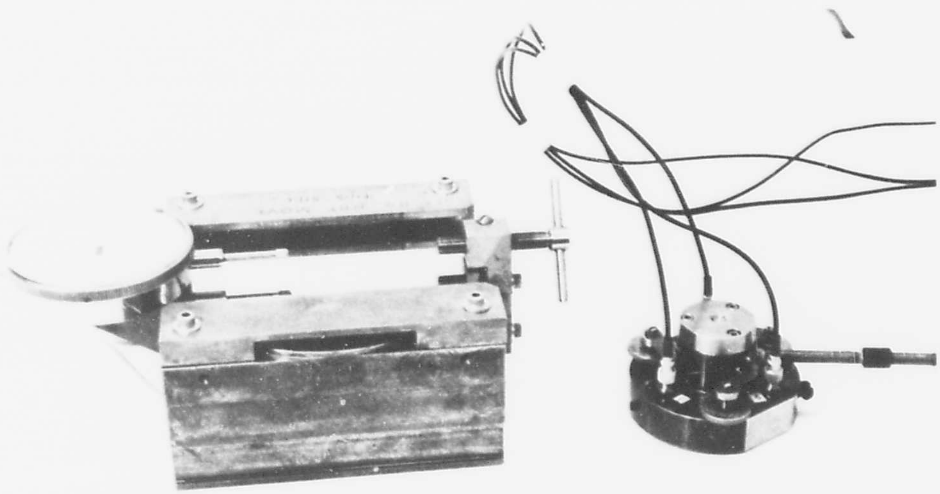

FIG. 3 : UPPER AND LOWER BEARING BLOCKS

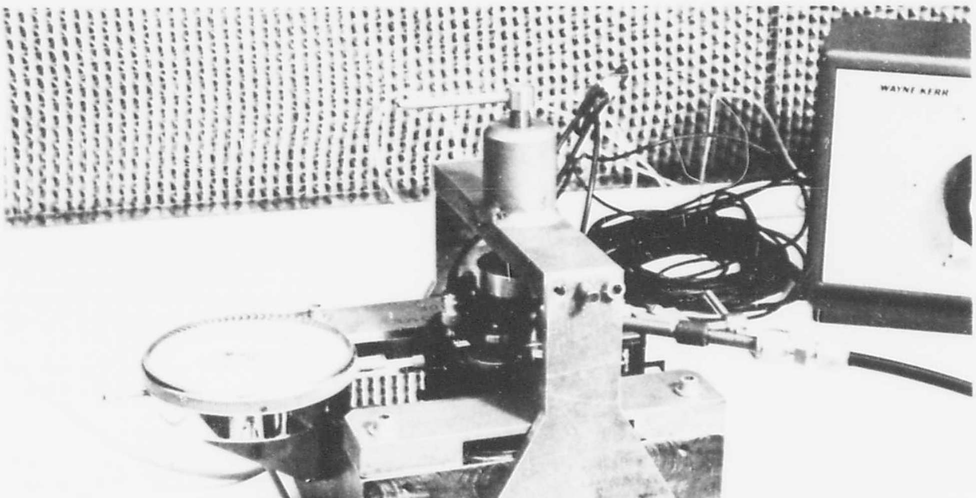

FIG. 4a : FEEDING HOLE TEST ASSEMBLY

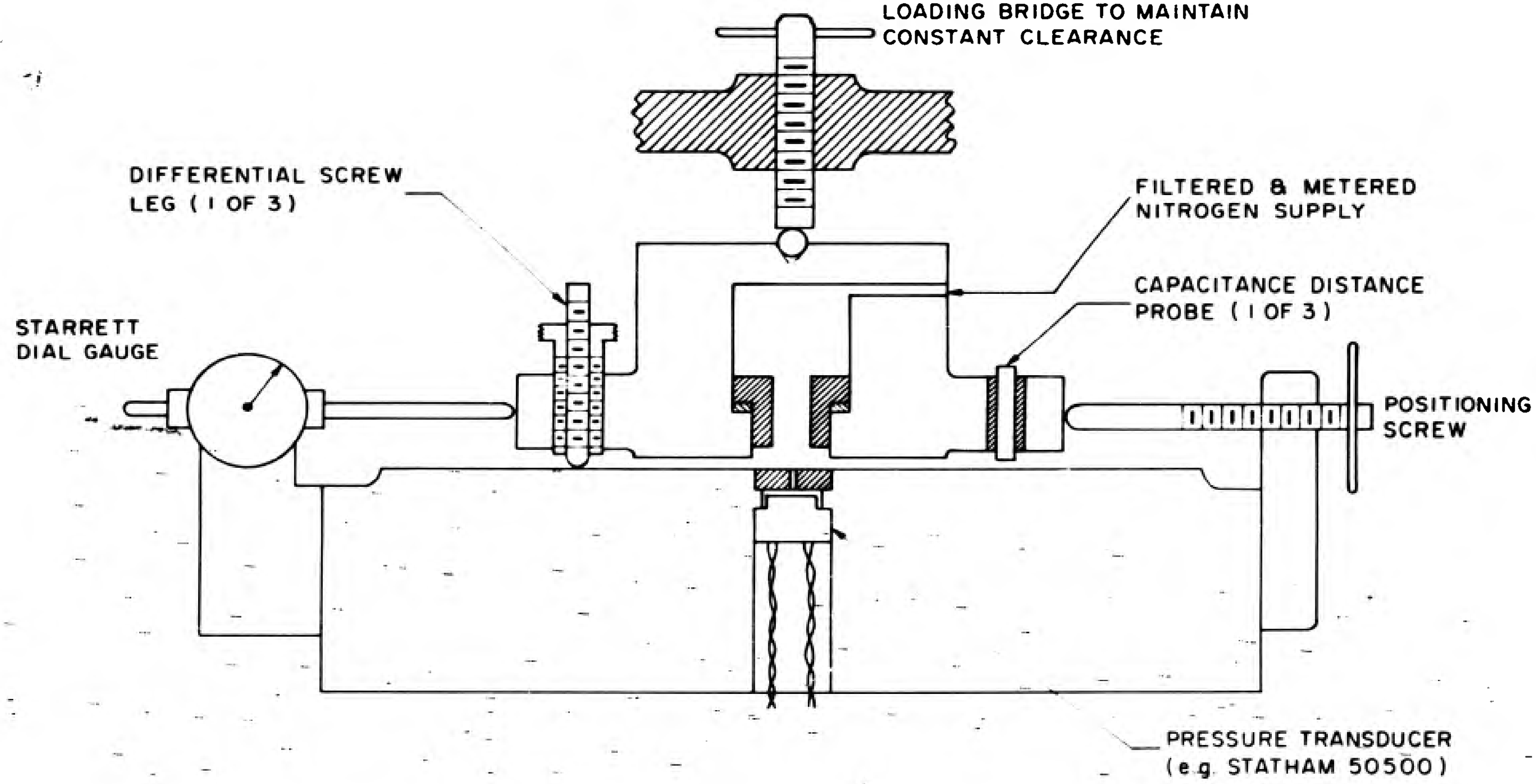

FIG. 4b : DIAGRAM OF FEEDING HOLE TEST ASSEMBLY

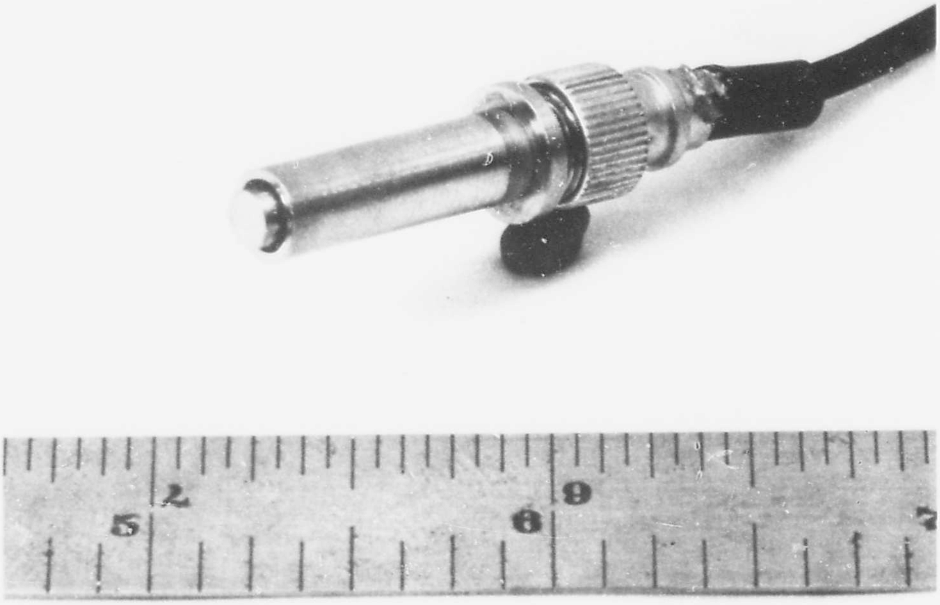

FIG. 5 : CAPACITANCE-TYPE DISTANCE MEASURING PROBE

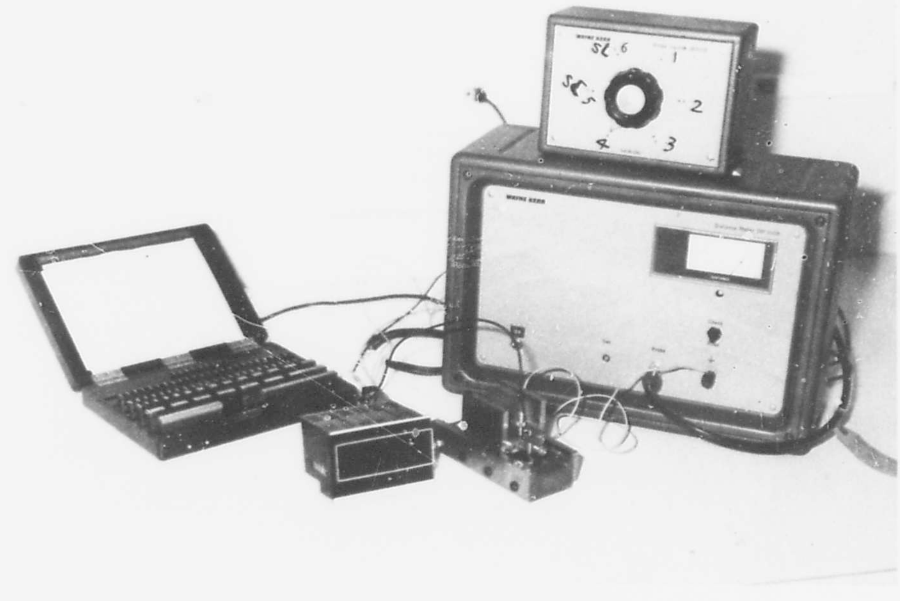

FIG. 6 : PROBE CALIBRATION SET-UP

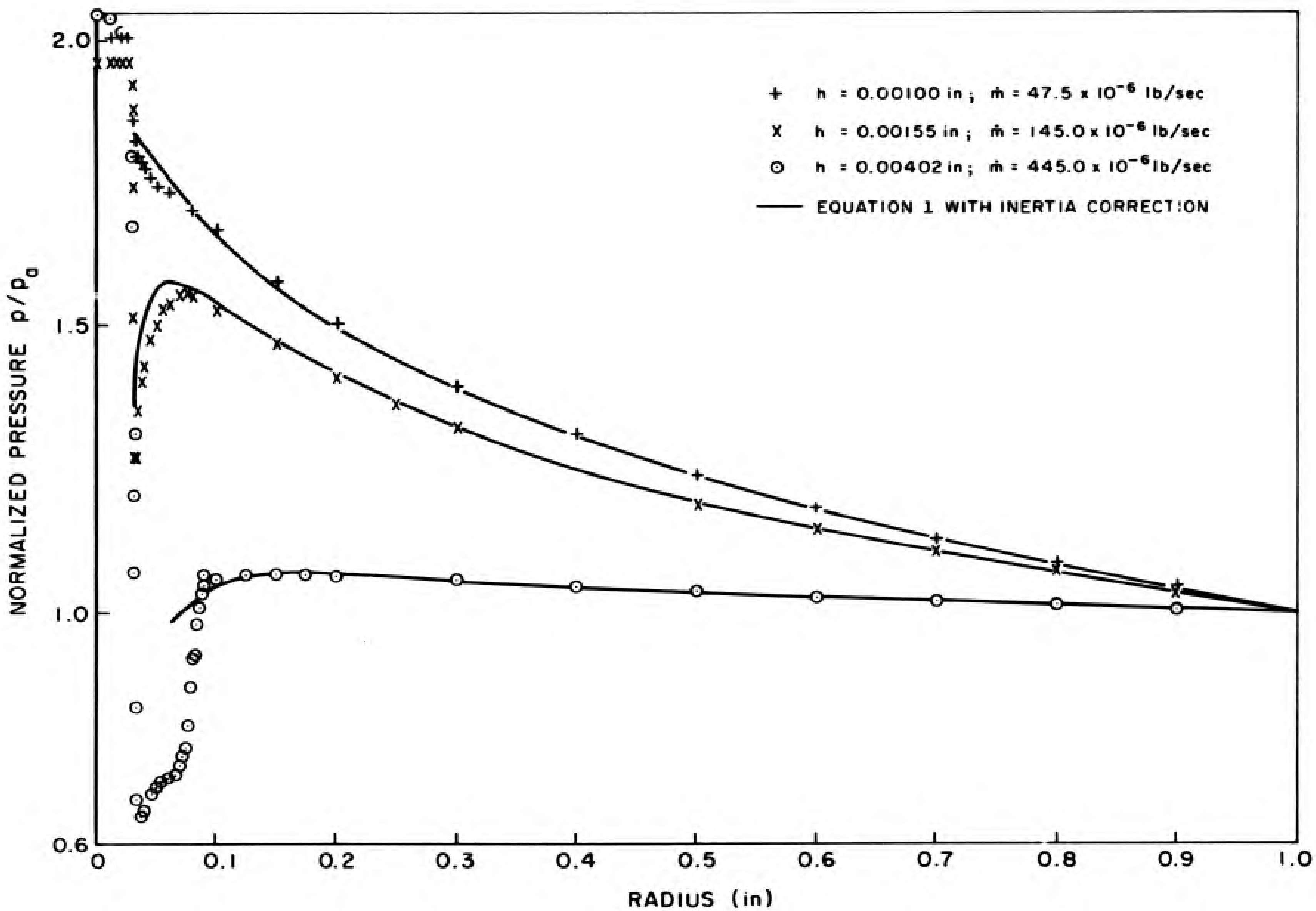

FIG. 7 : PRESSURE DISTRIBUTION CURVES FOR $R_S = 0.0313$ AND $P_S = 2.0$

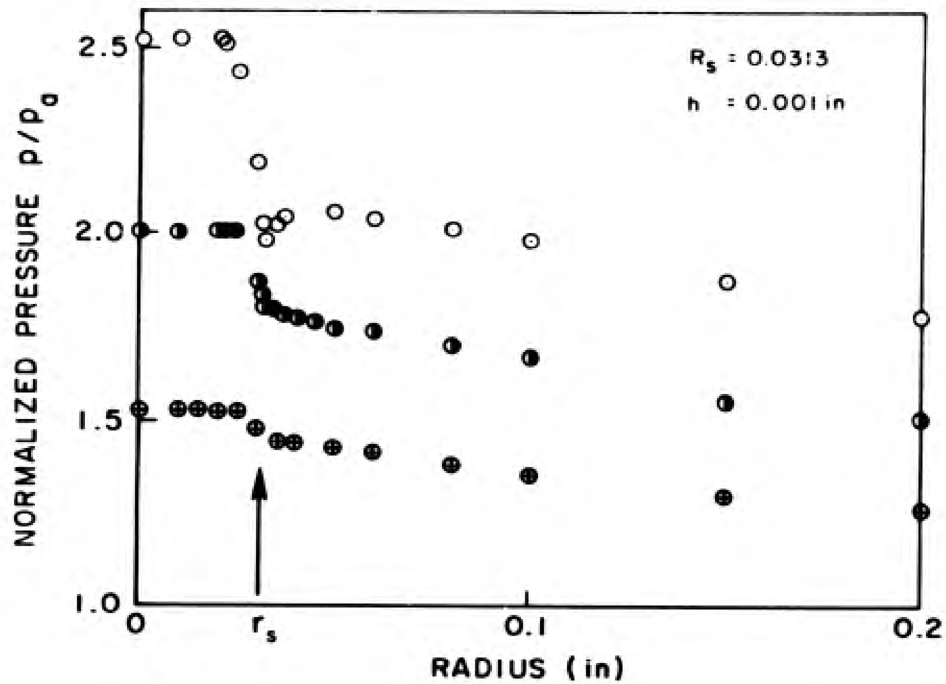

FIG.8 : EFFECT OF SUPPLY PRESSURE ON PRESSURE DISTRIBUTION

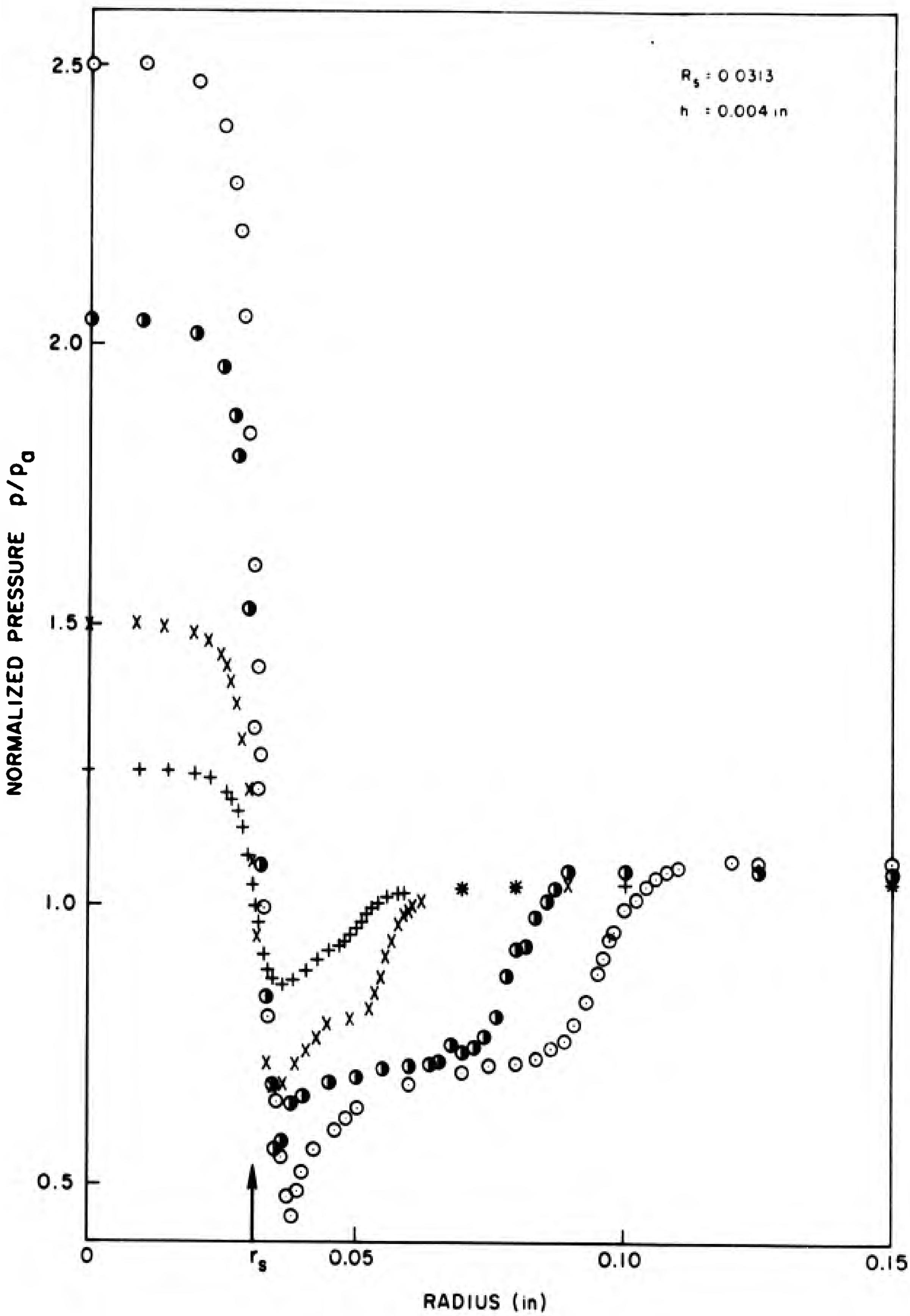

FIG.9 : EFFECT OF SUPPLY PRESSURE ON PRESSURE DISTRIBUTION

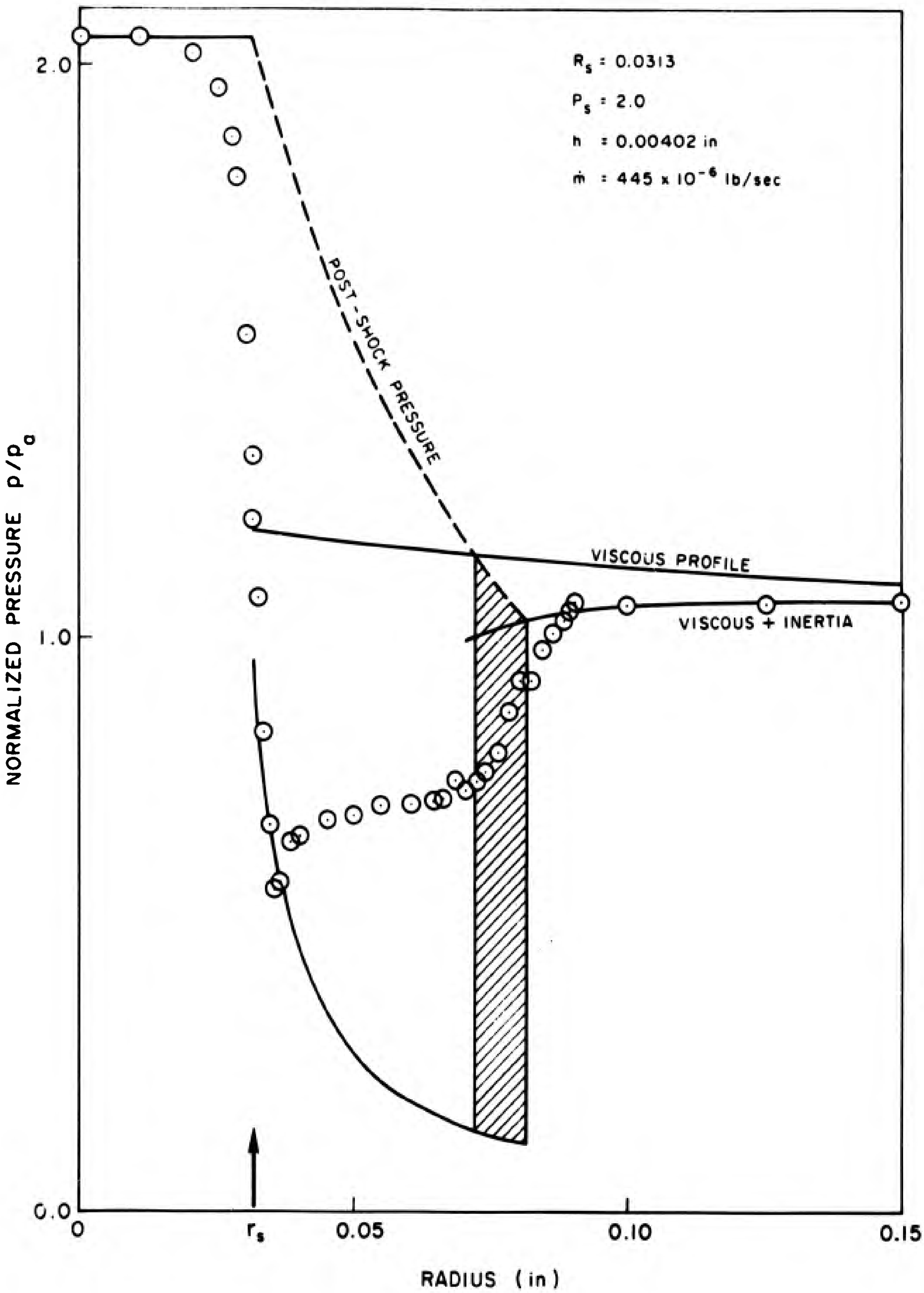

FIG. 10 : SHOCK POSITION IN CLEARANCE SPACE

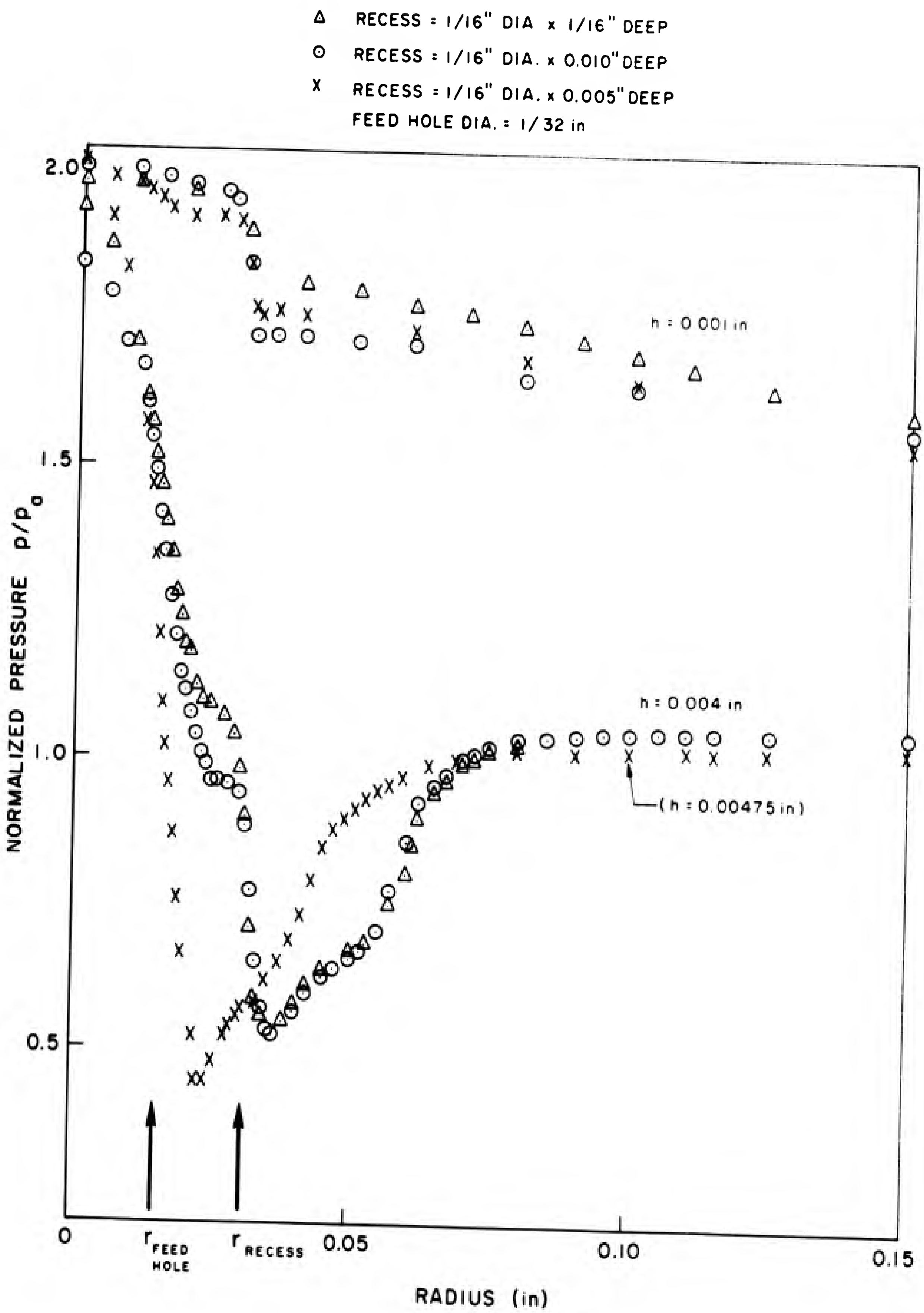

FIG. 11 : EFFECT OF RECESS DEPTH ON PRESSURE DISTRIBUTION

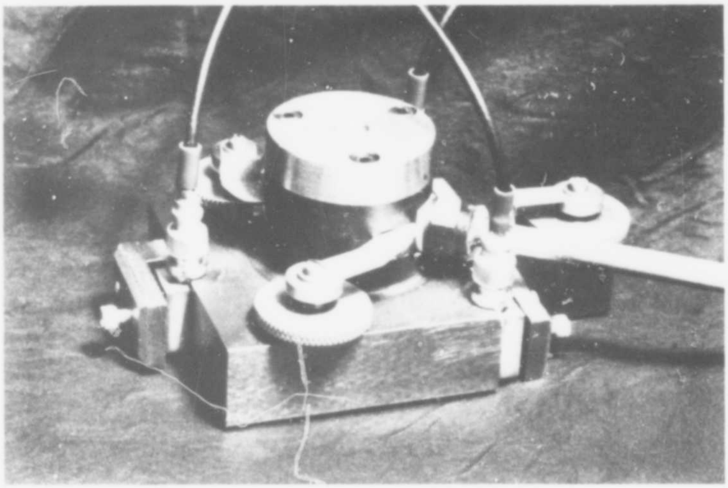

FIG. 12a : LARGE RADIUS RATIO BEARING BLOCK

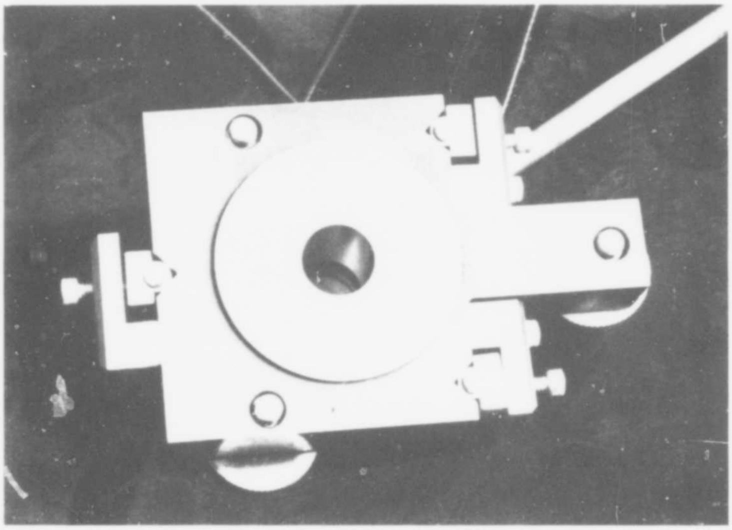

FIG. 12b : VIEW OF BEARING SURFACE, SUPPLY HOLE AND CAPACITANCE PROBES

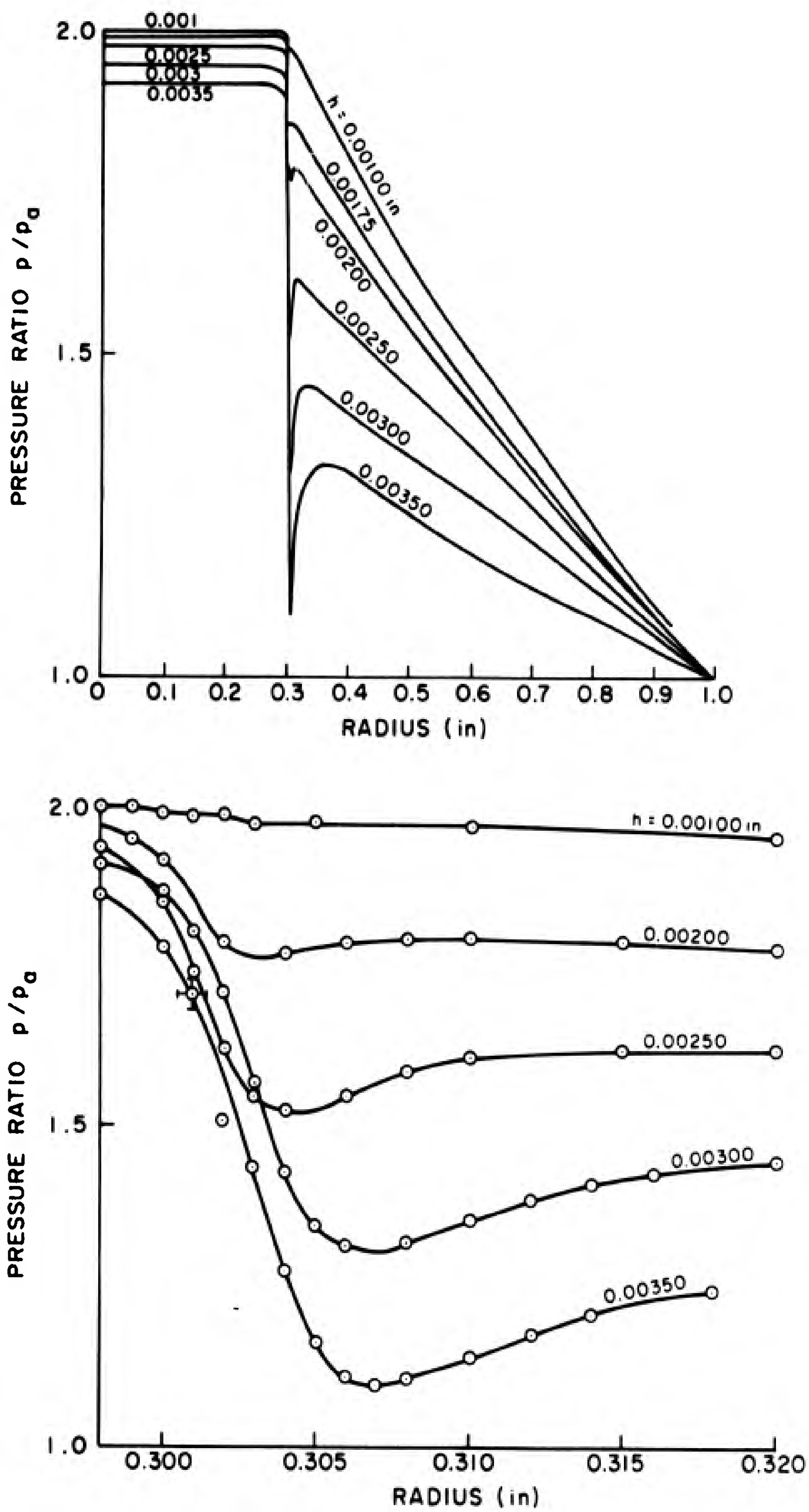

FIG. 13: PRESSURE DISTRIBUTIONS FOR $R_s = 0.3$ AND $P_s = 2.0$

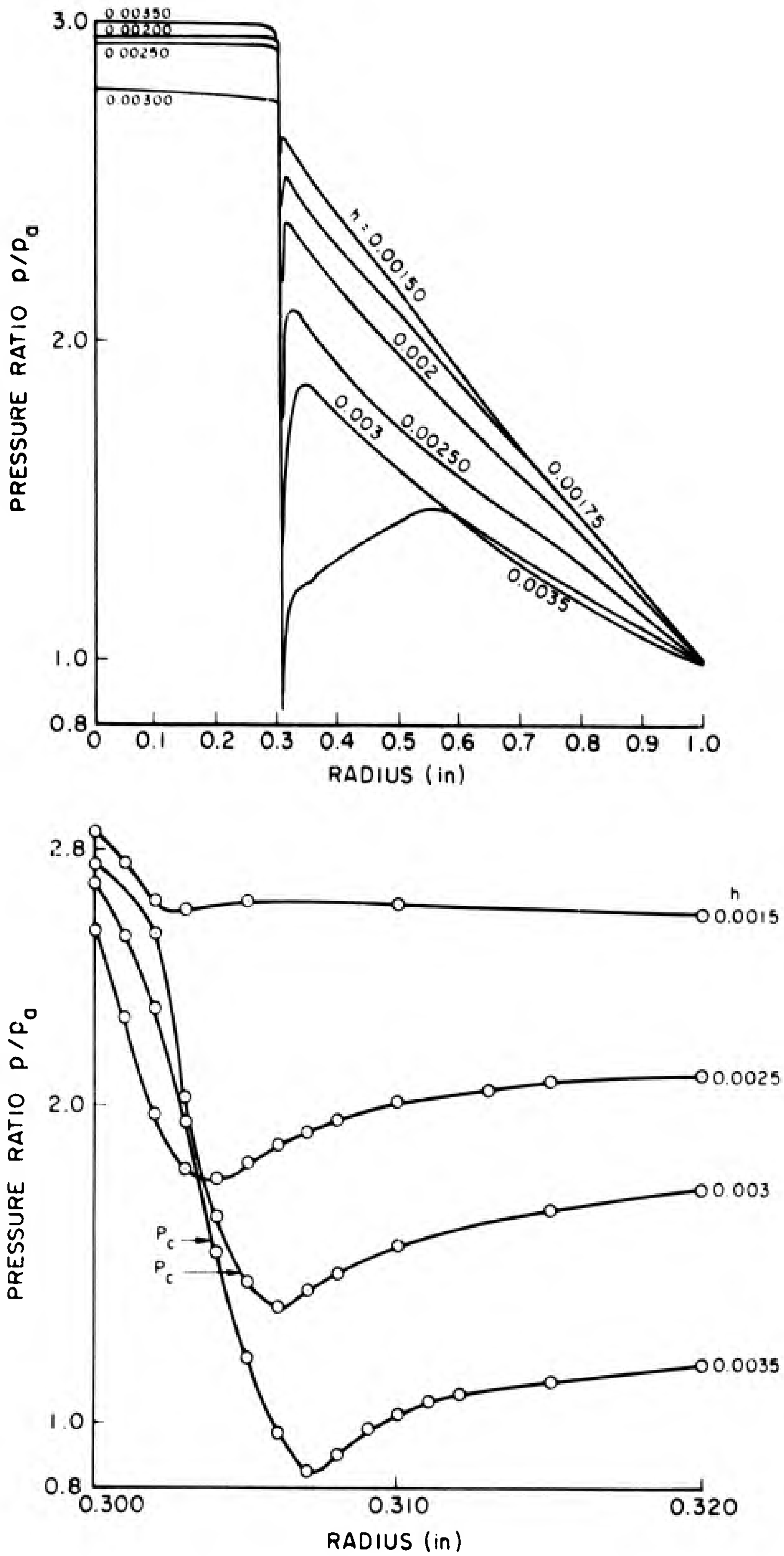

FIG. 14 : PRESSURE DISTRIBUTIONS FOR $R_s = 0.3$ AND $P_s = 3.0$

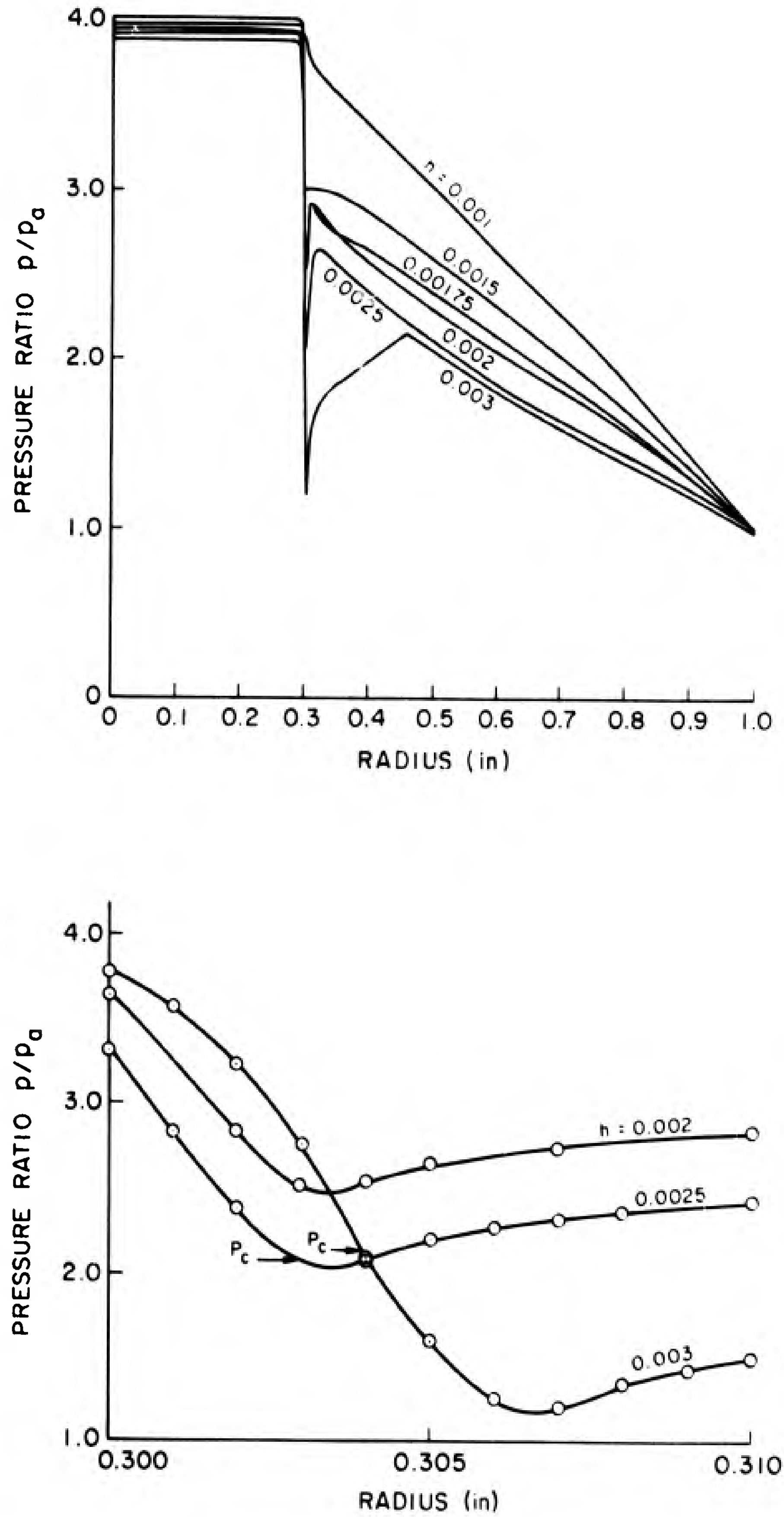

FIG. 15 : PRESSURE DISTRIBUTIONS FOR $R_s = 0.3$ AND $P_s = 4.0$

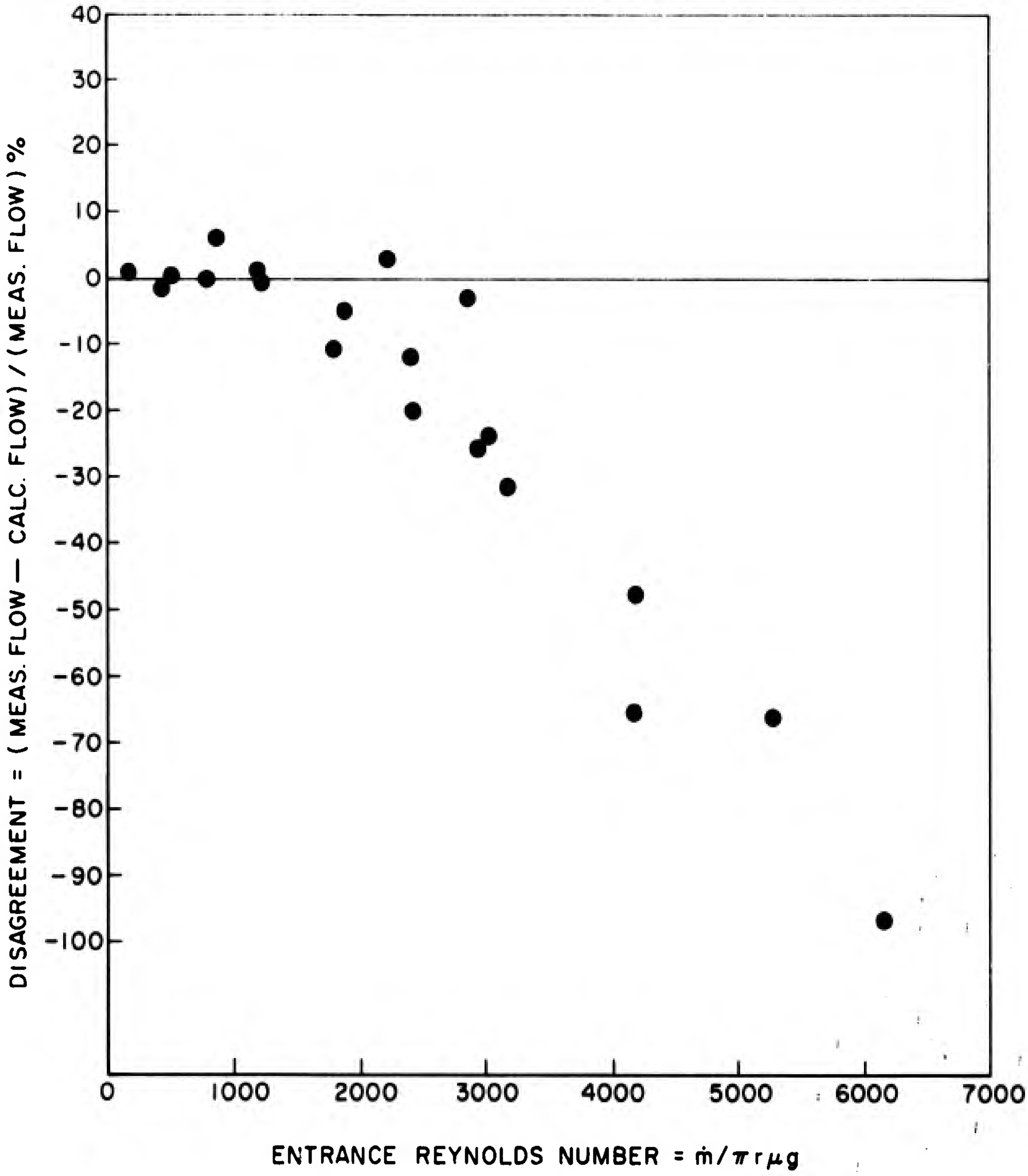

FIG.16 : COMPARISON OF CALCULATED AND MEASURED FLOW RATES FOR BEARING WITH $R_s = 0.3$

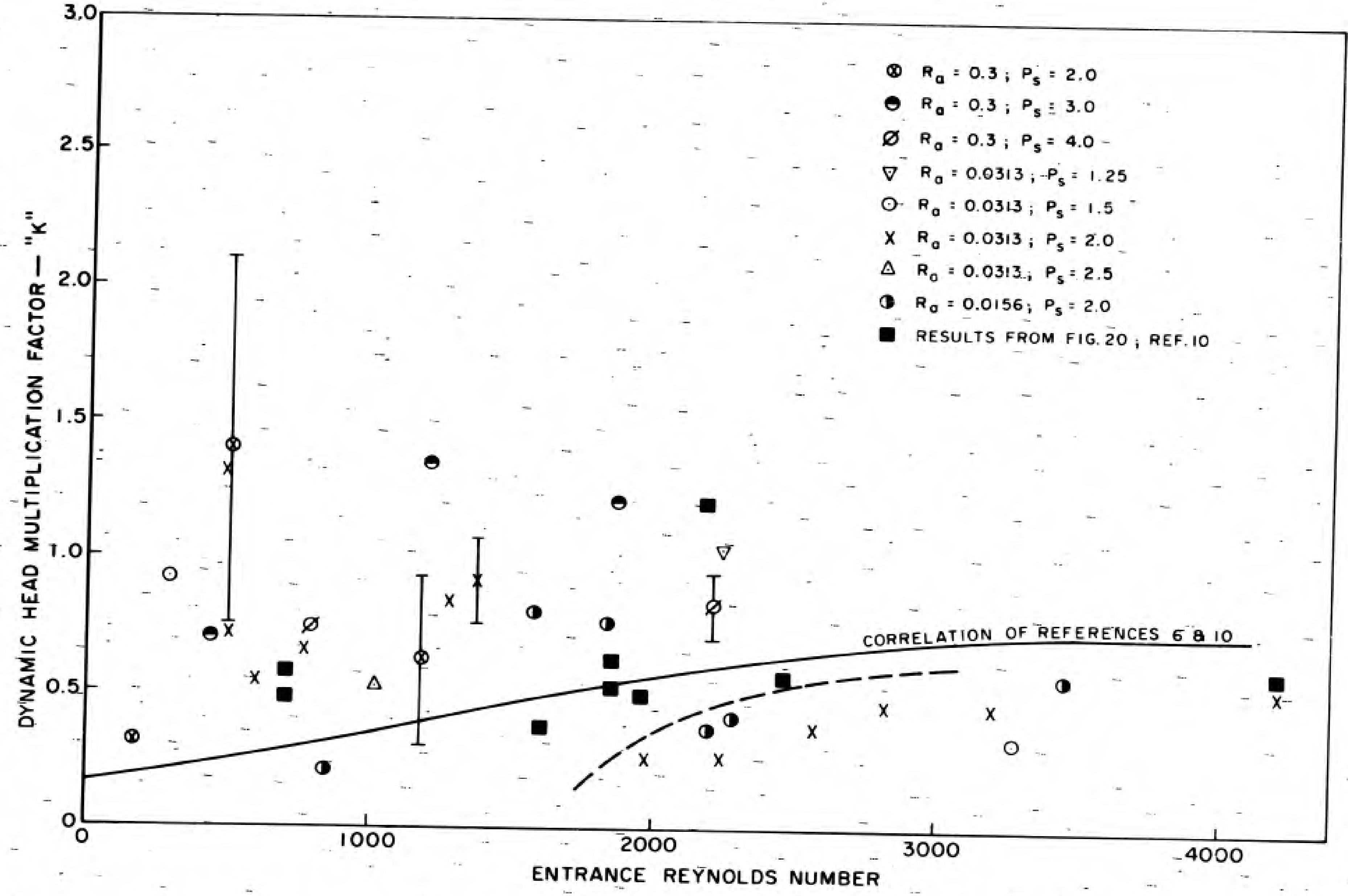

FIG. 17 : DYNAMIC HEAD FACTOR AS A FUNCTION OF ENTRANCE REYNOLDS NUMBER

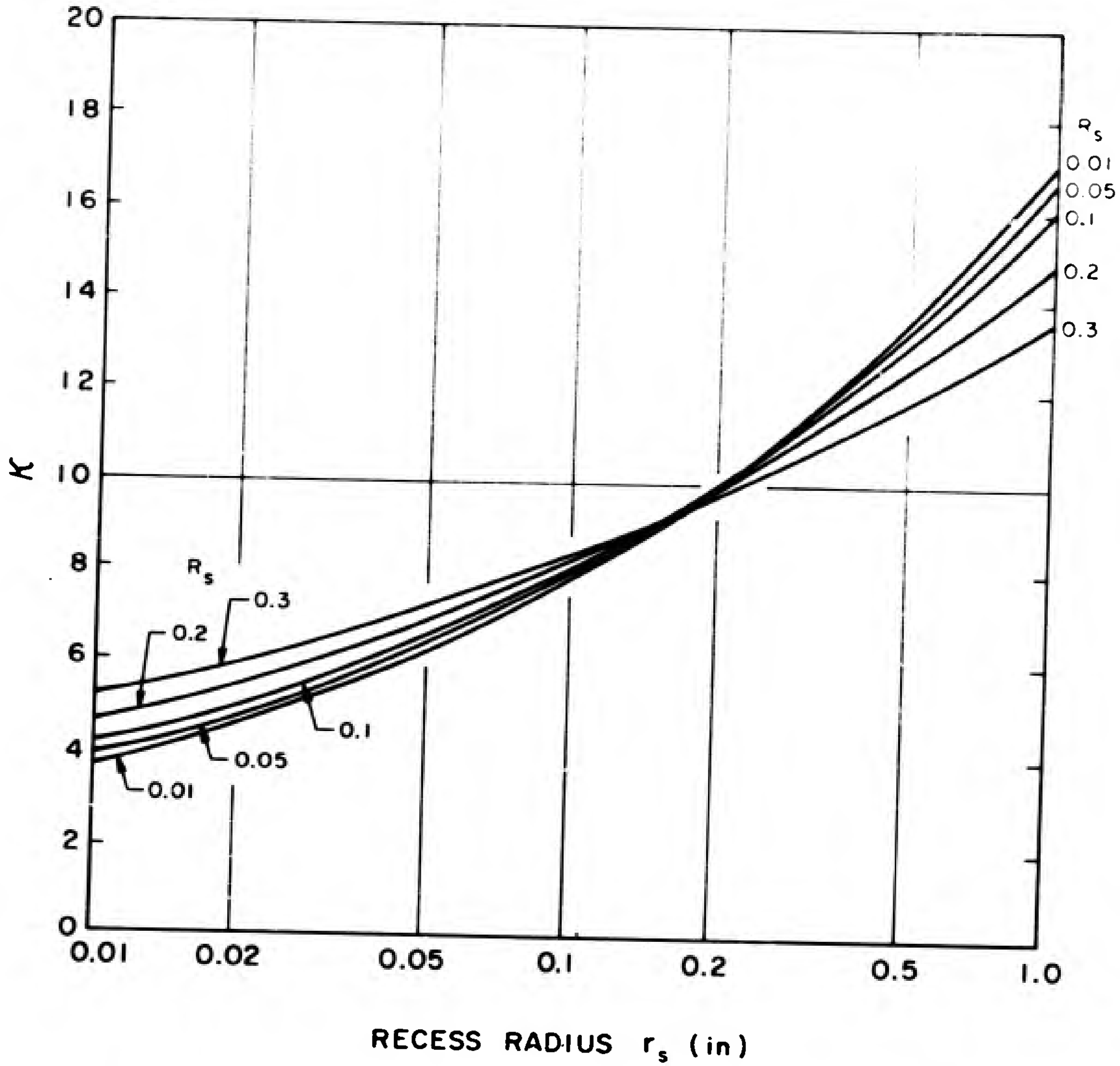

FIG. 18: EFFECT OF RADIUS RATIO AND INLET RADIUS ON INHERENT DISCHARGE COEFFICIENT FACTOR

BEARING DIA. = 2.0 in ; SUPPLY-HOLE DIA. = 0.0625 in
SUPPLY PRESSURE RATIO = 2.0
O - LOAD (lb) FROM INTEGRATED PRESSURE DISTRIBUTION
● - MEASURED FLOW RATE (cu in/sec)

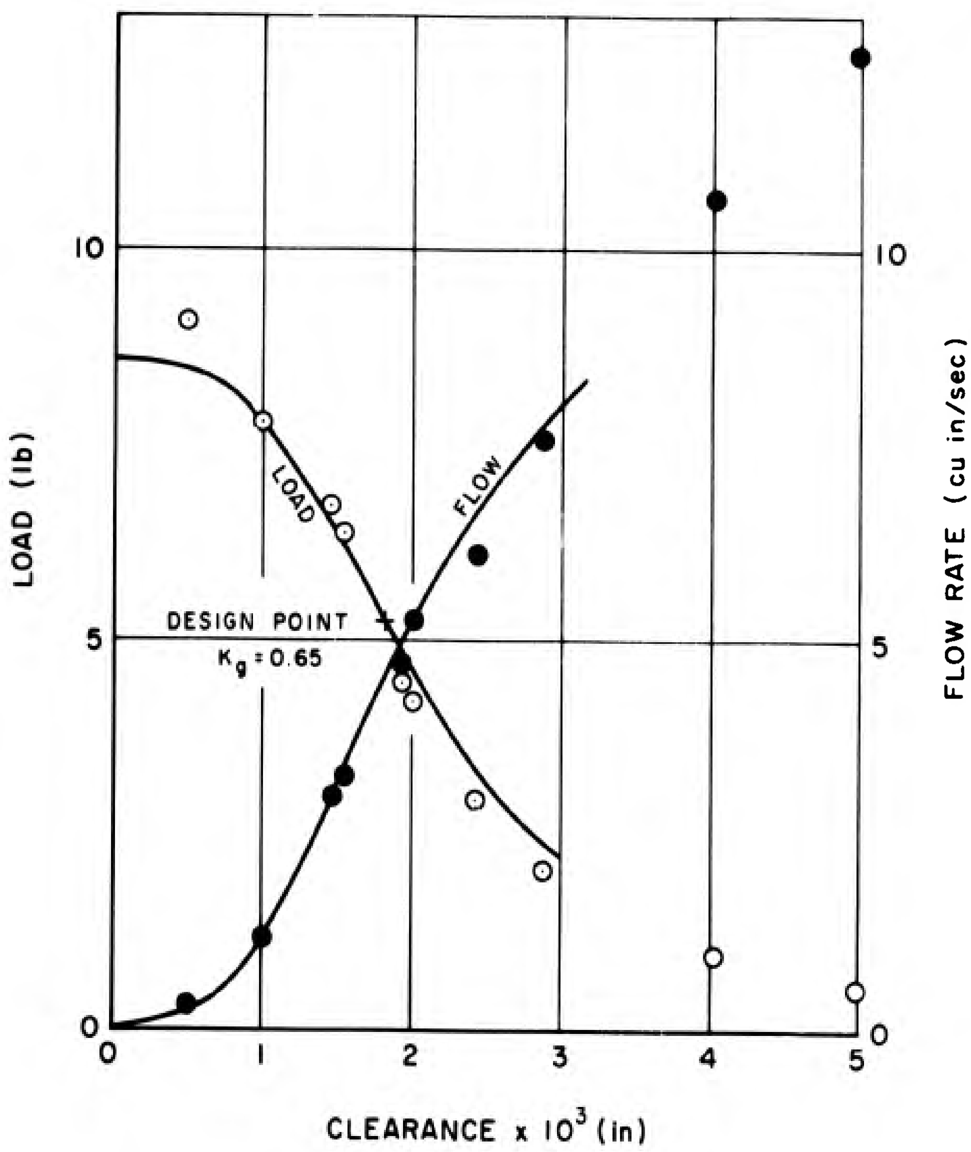

FIG. 19 : COMPARISON OF EXPERIMENTAL AND THEORETICAL LOAD AND FLOW CURVES

APPENDIX A

FORTRAN IV LEVEL G PROGRAM

FOR THRUST BEARING FEEDER HOLE TEST DATA ANALYSIS

```
C
C
C      THRUST BEARING FEEDER HOLE TEST DATA ANALYSIS
C
C
C       ALL PERMANENT OPERATIONAL CARDS IN FOLLOWING PROGRAMME ARE WHITE
C       ALL VARIABLE DECISION POINTS AND ATTACHED COMMENT CARDS ARE PINK
C       ALL JOB SUBMISSION CARDS ARE ORANGE
C       J IS RUN COUNTER USED IN ARRAY SUBSCRIPTS AND CUTOFF
C       J ASSUMES VALUE OF NUMBER OF DATA SET (RUN NO.) PRESENTLY BEING
C       PROCESSED
C       IF J NOT ORIGINALLY SET .EQ. ONE ALL DECISION PTS AFFECTED
C       ALL ARRAYS INVOLVING J MUST BE DIMENSIONED IN THE APPROPRIATE
C       SUBSCRIPT AT A VALUE .GE. THE NO. OF DATA SETS (RUNS) INVOLVED
C       FOR EACH JOB DECISION POINTS INVOLVING J MUST BE ADJUSTED TO BE
C       APPROPRIATE TO THE NUMBER OF DATA SETS TO BE PROCESSED
        J=1
C      NOTE THAT THE DIMENSION OF PA LIMITS  NUM  TO 7
C      GAUGE IS THE PRESSURE TRANSDUCER CONSTANT  (MV/PSI)
       READ (1,22) NUM, GAUGE
    22 FORMAT (I2,F8.5)
C       DIMENSION OF ARRAY PA .GE. NO. OF RUNS
        DIMENSION  PA(7)
    30  HPEN=0.0
        IF(J.NE.1) GO TO 90
        XINC=1./2.54
        YINC=1./2.54
        DIMENSION XPAR(2)
        DIMENSION YPAR(2)
        XPAR(1)=7.0
        XPAR(2)=38./2.54
        YPAR(1)=5.0
    14  YPAR(2)=25./2.54
        IND=1
        PEN=8.0
        CALL PSAVE(1000)
    90  CALL GRID (XINC,YINC,XPAR,YPAR,IND,PEN)
        IF (J.NE.1) GO TO 100
        DIMENSION TEXT(39)
        DIMENSION PEXT (26)
        DIMENSION TEXP (3)
        DIMENSION PEXP(4)
        DIMENSION PXPAR (10)
        DIMENSION PYPAR (10)
        READ(1,20) (TEXT(I),I=1,39)
    20  FORMAT(20A4/19A4)
         READ(1,21) (PEXT(I),I=1,26)
    21  FORMAT(20A4/6A4)
        READ(1,51)(TEXP(I),I=1,3)
    51  FORMAT(3A4)
        READ(1,52)(PEXP(I),I=1,4)
    52  FORMAT(4A4)
   100  ICOUNT=154
        PXPAR(1)=5.0
        PXPAR(2)=20.0
        PXPAR(7)=2.0-.25/2.54
        PXPAR(8)=.25/2.54
        PXPAR(9)=1.0
        PYPAR(1)=3.0
        PYPAR(2)=12.0
        PYPAR(7)=1.0
```

```
      PYPAR(8)=0.0
      CALL PRINT2 (TEXT,ICOUNT,PXPAR,PYPAR)
      ICOUNT=12
      PXPAR(7)=8.0
      PYPAR(7)=0.0
      CALL PRINT2(TEXP,ICOUNT,PXPAR,PYPAR)
      ICOUNT=102
      PXPAR(9)=2.0
      PXPAR(7)=1.0
      PXPAR(8)=0.0
      PYPAR(7)=2.0-.25/2.54
      PYPAR(8)=.25/2.54
      CALL PRINT2 (PEXT,ICOUNT,PXPAR,PYPAR)
      ICOUNT=16
      PXPAR(7)=0.0
      PYPAR(7)=5.0
      CALL PRINT2(PEXP,ICOUNT,PXPAR,PYPAR)
    3 READ(1,4) PA(J)
    4 FORMAT(F8.0)
C    PA(J) IS THE ATMOSPHERIC PRESSURE IN MILLIMETERS OF MERCURY CORRECTED TO
C       ZERO DEGREES CENTIGRADE.
C     DIMENSION OF ARRAY PATM .GE. NO. OF RUNS
      DIMENSION PATM(7)
      PATM(J)=PA(J)*.019338+.006
      N=1
      I0=1
C     N IS A COUNTER FOR THE MEASUREMENTS IN EACH RUN (DATA SET)
C     ARRAYS IN SUBSCRIPT N MUST BE DIMENSIONED IN THE APPROPRIATE
C     SUBSCRIPT AT A VALUE .GE. NO. OF MEASUREMENTS MADE IN THE
C     LARGEST DATA SET
C     IN ARRAY DIMENSION (X,Y) X .GE. NO. MEASUREMENTS/RUN ( MAX. N)
C     IN ARRAY DIMENSION (X,Y) Y .GE. NO. RUNS (MAX. J)
      DIMENSION R(65,7),PRMV(65,7),PRG(65,7),PR(65,7),PRATIO(65,7)
    1 READ(1,2)R(N,J),PRMV(N,J)
    2 FORMAT(2F7.0)
C    R(N,J)  IS THE RADIUS IN INCHES AT WHICH THE CORRESPONDING PRESSURE
C       PRMV(N,J)  IN MILLIVOLTS WAS READ.
    6 PRG(N,J)=PRMV(N,J)/GAUGE
      PR(N,J)=PRG(N,J)+PATM(J)
      PRATIO(N,J)=PR(N,J)/PATM(J)
      IF(N.EQ.1) GO TO 70
      GO TO 80
   70 WRITE(3,71)
   71 FORMAT (1H1)
      WRITE(3,72)J
   72 FORMAT(12H RUN NUMBER= ,I2)
      WRITE(3,73)
   73 FORMAT(//67H  RADIUS      MVOLTS      GAUGE PRESS ABSOLUTE PRESS   -
     1PRESS RATIO  /)
80   WRITE(3,7)R(N,J),PRMV(N,J),PRG(N,J),PR(N,J),PRATIO(N,J)
7    FORMAT(2X,F7.5,5X,F8.4,5X,F7.4,7X,F7.4,8X,F7.4 )
      IF (R(N,J).GE.1.0) GO TO 8
      N=N+1
      IF(R(N-1,J).GT..38) GO TO 10
      I0=I0+1
      DIMENSION XPPAR(6),YPPAR(5)
   10 GO TO 1
8     SUPP=PR(1,J)
     CALL BLOAD(PRG,R,J)
     CALL BELOW(PATM,J,SUPP,GAUGE)
      XPPAR(1)=7.0
      XPPAR(2)=38./2.54
```

```
      XPPAR(3)=0.
      XPPAR(4)=2.54/100.
      XPPAR(5)=18.0
      YPPAR(1)=5.0
   13 YPPAR(2)=25./2.54
      YPPAR(3)=0.
      YPPAR(4)=0.254
      YPPAR(5)=HPEN
      CALL POINT(R(1,J),PRATIO(1,J),10,XPPAR,YPPAR)
      HPEN=HPEN+1.0
      J=J+1
C     PLOT CHANGED IF J EQUAL TO THE NUMBER OF FIRST RUN OF NEW GROUP
      IF(J.EQ.6) GO TO 40
      GO TO 41
   40 CALL PAGE
      GO TO 30
   41 CONTINUE
C     CUTOFF OCCURS IF RUN COUNTER (J) .GT. NO. OF RUNS
      IF (J.GT.NUM) GO TO 9
      GO TO 3
    9 CALL PEND
     STOP
       END
```

```
C       SUBROUTINE  LOAD TO INTEGRATE PRESSURE DISTRIBUTION
        SUBROUTINE BLOAD(PRG,R,J)
        DIMENSION  PRG(65,7),R(65,7),PPRG(65,7)
        SUM=0
        N=1
  250   IF  (R(N,J)-1.0) 260,290,290
  260   IF (R(N+1,J)-R(N,J)-.01) 280,280,270
  270   S=(PRG(N+1,J)-PRG(N,J))/(R(N+1,J)-R(N,J))
        DLOAD = 3.14159*(PRG(N,J)-S*R(N,J))*(R(N+1,J)**2.-R(N,J)**2.)
       1+2.0944*S*(R(N+1,J)**3.-R(N,J)**3.)
        SUM =SUM + DLOAD
        N = N + 1
        GO TO 250
  280   PPRG(N,J) = (PRG(N,J) + PRG(N+1,J))/2.
        AREA = 3.14159*(R(N+1,J)*R(N+1,J)-R(N,J)*R(N,J))
        SUM = SUM + PPRG(N,J)*AREA
        N=N+1
        GO TO 250
  290   WRITE(3,295)
        WRITE(3,300) SUM
  295   FORMAT(1H0)
  300   FORMAT (17H  LOAD CAPACITY =,F10.3,8H POUNDS )
        RETURN
        END
```

```
C       SUBROUTINE "FLOW"  TO CALCULATE FLOW AND BEARING PARAMETERS
        SUBROUTINE BFLOW(PATM,J,SUPP,GAUGE)
        REAL*4 KG
        DIMENSION PATM(7),PRMV(5),PRG(5),PR(5),PRR(5),R(5)
        DIMENSION PSUPP(5),PSG(5),PS(5),FLOW(5),AREA(5),WSPEC(5)
        DIMENSION QFLOW(5),WFLOW(5),WMEAS(5),QCORR(5),WCORR(5)
        DIMENSION  XCOF(7),COF(7),ROOTR(7),ROOTI(7)
        READ(1,5) TEMPC,TEMFC,CLEAR,RIN,PAMB
C       TEMPC  IS THE ROOM TEMPERATURE IN DEGREES CENTIGRADE
C        TEMFC  IS THE FLOWRATOR GAS TEMPERATURE IN DEGREES CENTIGRADE,
C        AVERAGED OVER THE RADIUS RANGE 0.4  TO  0.8  INCHES
C       CLEAR  IS THE BEARING CLEARANCE  ( INCHES )
C       RIN IS THE RADIUS OF THE FEEDING RECESS IN INCHES
C       PAMB  IS THE STATIC PRESSURE AT THE EXTREME RADIUS (MILLIVOLTS)
    5   FORMAT(2F5.2,3F10.6)
        DENS = 13.596-.002457*TEMPC
        TEMPR=491.7+1.8*TEMPC
        TEMFR=491.7+1.8*TEMFC
        PAMB = PATM(J) + PAMB/GAUGE
        SUM1=0.0
        SUM2=0.0
        DO 100 I=1,5
        R(I) = (13.0 + FLOAT(I))/20.0 -.005
```

```
C      THE FOLLOWING VALUES ARE TO BE READ IN FOR THE RADII 0.695,.745,.795,.845,.895
C      PRMV(I)  IS THE PRESSURE AS MEASURED IN MILLIVOLTS
C      PSUPP(I)  IS THE SUPPLY PRESSURE IN INCHES OF MERCURY
C      FLOW(I)  IS THE MEASURED BUT UNCORRECTED GAS FLOW RATE IN POUNDS PER
C         SECOND.   THE CORRECTION FOR PRESSURE AND TEMPERATURE ARE MADE WITHIN
       READ(1,10) PRMV(I),PSUPP(I),FLOW(I)
 10    FORMAT(2F10.4,F10.7)
 55    PRG(I)=PRMV(I)/GAUGE
       PR(I)=PRG(I)+PATM(J)
       PSG(I)=PSUPP(I)*DENS*.03613
       PS(I)=PSG(I)+PATM(J)
       WSPEC(I)=.00151*SUPP/TEMPR
       WMEAS(I)=FLOW(I)*SQRT(36.05*PS(I)/TEMPR)
       AREA(I)=6.283*R(I)*CLEAR
 60    DELPP=0.6*WMEAS(I)*WMEAS(I)*SUPP/(386.2*WSPEC(I)*PR(I)*AREA(I)
      1*AREA(I))
       PR(I) = PR(I) + DELPP
 75    QCORR(I) = 0.10124E+09*(CLEAR**3.)*(PR(I)*PR(I)-PAMB*PAMB)/-
      1(SUPP*ALOG(1./R(I)))
       WCORR(I)=QCORR(I)*WSPEC(I)
       SUM1=SUM1+WCORR(I)
       SUM2=SUM2+WMEAS(I)
 100   CONTINUE
       AVER1=SUM1/5.
       AVER2=SUM2/5.
       ERROR=(AVER2-AVER1)*100./AVER2
       WRITE(3,110) AVER1,AVER2,ERROR
 110   FORMAT(/2X,'AV. CALC. FLOW=',E14.5,8X,'AV. MEAS. FLOW=',E14.5,
      11X,'LBS./SEC.',8X,'ERROR=',F6.1,'%')
       PI = SQRT(PAMB*PAMB+(9.8778E-09*SUPP*AVER2*ALOG(1./RIN))/-
      1(WSPEC(5)*(CLEAR**3.)))
       RPI=PI/PATM(J)
       DIFF=SUPP-PI
       KG=(PI-PATM(J))/(SUPP-PATM(J))
       RE=0.31856E+06*AVER2/RIN
       RATIO=PI/SUPP
       WRITE(3,121)  RPI,RATIO,DIFF
 121   FORMAT(/2X,'PI/PA=',F6.4,8X,'PI/PS=',F6.4,8X,'(PS-PI)=',F6.3)
       IF(RATIO-1.0) 125,190,190
 125   IF(RATIO-0.528) 130,135,135
 130   RATIO=0.528
 135   ARG=RATIO**1.429-RATIO**1.713
       CD=AVER2/(8420.*WSPEC(5)*RIN*CLEAR*SQRT(TEMPR)*SQRT(ARG))
       WRITE(3,120) PI,KG,RE,CD
 120   FORMAT(/2X,'PI=',F6.2,8X,'KG=',F5.3,8X,'FILM ENTRANCE REYNOLDS NO.
      1=',F6.0,9X,'EQUIV ORIFIC. COEFF.   CD=',F5.3)
C
C
C      SUBROUTINE POLRT IS USED TO DETERMINE MACH NUMBER AT ENTRANCE TO GAP
C
C
       M=6
       CONST=0.1927*AVER2*(TEMPR**0.5)/(RIN*CLEAR*SUPP)
       XCOF(1)=125.0
       XCOF(2)=-137.1/CONST
       XCOF(3)=75.0
       XCOF(4)=0.0
       XCOF(5)=15.0
       XCOF(6)=0.0
```

```
      XCOF(7)=1.0
      CALL POLRT(XCOF,COF,M,ROOTR,ROOTI,IER)
      WRITE(3,140) IER
  140 FORMAT(////2X,'IER=',I2)
      WRITE(3,145)
  145 FORMAT(//3X,'REAL ROOTS',10X,'IMAG ROOTS')
      DO 160 I=1,6
      WRITE(3,150) ROOTR(I),ROOTI(I)
  150 FORMAT(3X,F9.4,11X,F9.4)
  160 CONTINUE
      DRAT1=0.52828*((1.2/(1.+0.2*ROOTR(1)*ROOTR(1)))**3.5)
      DRAT2=0.52828*((1.2/(1.+0.2*ROOTR(2)*ROOTR(2)))**3.5)
      PE1=DRAT1*SUPP
      PE2=DRAT2*SUPP
      PDYN1=SUPP-PE1
      PDYN2=SUPP-PE2
      VOHR1=DIFF/PDYN1
      VOHR2=DIFF/PDYN2
      WRITE(3,180) PE1,PE2,PDYN1,PDYN2,VOHR1,VOHR2
  180 FORMAT(/2X,'PENT1=',F6.3,3X,'PENT2=',F6.3,3X,'PDYN1=',F6.3,3X,
     1'PDYN2=',F6.3,3X,'KVOHR1=',F6.3,3X,'KVOHR2=',F6.3)
  190 CONTINUE
      RETURN
      END
```

APPENDIX B

CALCULATION OF LOAD AND FLOW RATE FOR A CIRCULAR THRUST BEARING WITH A SINGLE CENTRAL INLET

The full derivation of the following equations can be found in Reference 14.

The load is given by

$$W = F_{WI} \, A \, p_a \, (P_o - 1)$$

where the load factor, F_{WI}, for inherently-compensated bearings can be related to that for the orifice-compensated case by

$$F_{WI} = F_{WO} + \frac{1 - Kg}{Kg} R_s^2$$

and

$$F_{WO} = \frac{R_s^2}{2} \cdot \frac{P_o}{P_o - 1} \cdot \exp(\sigma^2) \cdot \frac{\sqrt{\pi}}{\sigma} \left[\operatorname{erf}\sigma - \operatorname{erf}\frac{\sigma}{P_o} \right]$$

for viscous isothermal flow.

The volumetric flow rate is

$$Q = \frac{F_Q \, h^3 (P_o^2 - 1) \, p_a}{6\mu}$$

with

$$F_Q = \frac{1}{2 \log_e (1/R_s)}$$

The clearance is given by

$$h = \left[\frac{1}{\Lambda_{SI}} \cdot \frac{1}{\Phi_I} \right]^{0.694}$$

where Λ_{SI} is an inherently-compensated version of the well-known bearing restrictor coefficient modified by the use of equation (10); that is

$$\frac{1}{\Lambda_{S1}} = \sqrt{\frac{2k}{k-1}} \cdot \frac{P_o}{(P_o^2 - 1)^{0.8}} \cdot \sqrt{\left(\frac{P_o}{P_s}\right)^{\frac{2}{k}} - \left(\frac{P_o}{P_s}\right)^{\frac{k+1}{k}}}$$

and

$$\Phi_1 = \frac{p_o}{12\kappa\mu\sqrt{g\, R_g T_s}} \cdot \frac{F_Q}{r_s^{\,0.44}}$$

κ may be read from Figure 18.